Loofah activated carbon with hierarchical structures for high-efficiency adsorption of multi-level antibiotic pollutants

Zhe Wang[a], Guangjin Wang[e], Wenyao Li*[,a,c], Zhe Cui[d], Jianghong Wu[b], Isil Akpinar[c], Li Yu[b,*], Guanjie He[c], Junqing Hu[*,b]

[a]*School of Materials Engineering, Shanghai University of Engineering Science, Shanghai 201620, China.*

[b]*College of Health Science and Environmental Engineering, Shenzhen Technology University, Shenzhen 518118, China.*

[c]*Electrochemical Innovation Lab, Department of Chemical Engineering, University College London, London WC1E 7JE, UK*

[d]*State Key Laboratory for Modification of Chemical Fibers and Polymer Materials, College of Materials Science and Engineering, Donghua University, Shanghai 201620, China.*

[e]*School of Materials Science and Hydrogen Energy, Foshan University, Foshan 528000, P.R. China*

Corresponding Authors: wenyao.li@ucl.ac.uk (Wenyao Li); yuli@sztu.edu.cn (Li Yu); hujunqing@sztu.edu.cn (Junqing Hu)

ABSTRACT

For antibiotic contaminants, biochar adsorbents have been regarded as one of the most suitable materials due to their safety for human health and good adsorption performance. In this study, loofah activated carbon (LAC) was prepared by a simple high temperature carbonization process, while mixing LAC with agarose solution under stirring at 90 °C, after which LAC-loaded agarose aerogel (LAC-AA) adsorbents could be obtained by freeze-dried under a vacuum condition. The LAC is consisted of hierarchical laminae-trestle-laminae (L-T-L) microstructure with highly ordered, whose surfaces are fully covered by nanoscale protrusions. The unique hierarchical structures possessing high specific surface areas (~736.86 m^2 g^{-1}) and abundant active surface sites, which contribute significantly to the adsorption of antibiotics (to name a few, tetracycline (TC), ofloxacin (OFO) and norfloxacin (NFO)). The results indicate that the capacity of adsorption towards TC, NFO and OFO (1~40 ppm) by the LAC-loaded agarose aerogel (LAC-AA) adsorbents is 537.6, 434.8 and 581.4 mg g^{-1}, respectively, which is significantly greater than that of currently-available adsorbents. In parallel, the atomic adsorption model's simulation further confirms that the OFO is prone to be adsorbed on the LAC with the lowest adsorption energy that resulted in the largest adsorption capacity.

Keywords: Loofah activated carbon; Adsorption; Antibiotics; Multi-level pollutants.

1. INTRODUCTION

Antibiotics are potent medicines that have been used for several decades in both human beings and animals for the therapeutic treatment of infections and diseases.[1, 2] However, its water solubility makes the surrounding environments such as water, soil and food inevitably contaminated by antibiotics. With the developing of super-resistant bacteria, and the global antibiotics abuse thereof, antibiotic contamination has attracted increasingly concerns.[3] For most antibiotics, such as norfloxacin (NFO), ofloxacin (OFO) and tetracycline (TC), once they entered the body, the metabolic system can hardly eliminate them in a short period and the residues will accumulate in the body, resulting in bacteria tolerance.[4, 5] After excretion of antibiotics from body, they will remine almost unchanged in water bodies.[6] Therefore, the removal of antibiotics residues from polluted water is of significant importance for both human health and the aquatic environment. Moreover, low concentrations of antibiotics were reported to cause more serious hazards to human health and ecological environment than high concentrations of them.[7] Therefore, developing technologies and materials that are inexpensive and capable of removing antibiotic solutions in various concentration ranges with high efficiency is still a challenge.[8-10]

Generally, methods adopted to remove antibiotics from water mainly include biodegradation,[11] photocatalytic,[12] advanced oxidation, [13] electrochemical oxidation, [14] adsorption, [15] and so on. Among these technologies, adsorption exhibits distinctive advantages, such as easy operation process, low cost, high removal efficiency, and no toxicities generated from intermediates has been widely used for water treatment. [16, 17] The adsorbent materials, such as natural ore materials, metal oxides (e.g., zeolites, [18] SiO_2, [19] Al_2O_3, [20] Fe_2O_3, [21] $H_2Ti_2O_5 \cdot H_2O$ nanobelts and magnetite nanocomposite, [22, 23] and carbon nanomaterials have been studied for the adsorption of antibiotics. Note that the capacity of adsorption is closely linked with specific surface area of materials and structures, for instance, zeolite is a porous adsorbent, its adsorption capacity towards TC is found to be of 27.78 mg g^{-1}, [24] while modified mesoporous zeolite composites demonstrate a greater adsorption capacity of 186.09 mg g^{-1} due to its

increased specific surface area.[25] Therefore, carbon-based materials have become an intense study object for adsorption studies because of the excellent specific surface area. These materials include carbon nanotubes (CNTs),[26] graphene,[27] active carbon and biological activated carbon (BAC), [28, 29] among which graphene and graphene composite materials have received great attention arising from their fine chemical resistance and outstanding mechanical properties.[27, 30] However, nanoscale graphene is also reported to have toxicological effects on different cell lines of plants, animals, and even human beings.[31] In this scenario, BAC is being concerned by researchers due to its harmlessness to the human body as well as carbon sequestration on basis of unique characteristics of the physicochemical surface, as high hydrophobicity and high specific surface area, developed pore structure.[32, 33] There are many natural single structures and artificially assembled multi-structure biological activated carbon adsorbents, such as Human hair-derived biochar for tetracycline,[34] the Pinus taeda-derived activated biochar for the adsorption of tetracycline[35], g-MoS_2 decorated biochar nanocomposites of tetracycline.[36] These studies indicate that the adsorbent materials with composite structure have better performance than the single-structure bioactive carbon. Therefore, there is an increasing demand for developing safe and non-toxic composite adsorbents with a composite structure and high specific surface area via easy and green methods.

In this study, loofah activated carbon (LAC) from natural loofah sponge was acquired by high temperature carbonization, while put LAC in agarose solution with stirring at 90 °C as precursor to obtain LAC-loaded agarose aerogel (LAC-AA) adsorbents by freeze-dried under a vacuum condition. According to the result illustrations of BET and SEM, the LAC exhibit high specific surface area and highly ordered hierarchical laminae-trestle-laminae (L-T-L) microstructure, which the surface are fully covered by nanoscale protrusions. The unique structures and large specific surface areas of LAC-AA are the basis of exploring the behavior and performance for adsorbing three different antibiotics. A series of adsorption experiments were conducted by using NFO, OFO, TC solutions as the model antibiotics on LAC-AA adsorbents. In addition, the atomic adsorption model's simulation also carried out to explain the relationship

between the adsorption energy with adsorption capacity.

2. EXPERIMENTAL SECTION

2.1 Preparation of the LAC

The LAC was obtained by the carbonization of loofah (Figure 1a) in a tube furnace. Argon was used as a protective gas, the temperature was raised to 800 °C at a rate of 2 °C min^{-1} and kept for 6 h, then waiting the temperature decrease to room temperature (Figure 1b).

2.2 Preparation of the LAC-AA adsorbent

Firstly, 400 mg of agarose (gelling point of ~36 °C) was dissolved in 50 mL deionized water at 90 °C under stirring, then 125 mg of the as-obtained LAC powder was poured into the agarose solution with vigorous stirring, keeping for 6 h. The LAC-loaded agarose hydrogel was obtained by 5 h storage of the mixture in a refrigerator (Figure 1c, e). Afterward, the hydrogel was freeze-dried on a freeze-dryer under a vacuum condition at a temperature of -50 °C for 48 h. Finally, a lightweight and compressible biosorbent was obtained (Figure 1 d, f, g). For comparison, agarose hydrogel without loading LAC was also prepared under the same conditions, presented in Figure S1 (in Supporting information).

2.3 Characterizations

The morphology of the as-prepared samples was examined by a Field-Emission Scanning Electron Microscope (FESEM, Hitachi, S-4800). The components of the products were characterized by a D/max-2550 PC X-ray diffractometer (XRD, Rigaku, Cu-Kα radiation). X-ray photoelectron spectroscopy (XPS) analysis tested the functional groups and the element state of adsorbents' surface. Characterize the structural integrity of the adsorbents by Raman spectroscopy (JOBIN-YVON T64000). The total specific surface area of the materials was determined making use of the

Brunauer-Emmett-Teller (BET) theory. BET specific surface area was calculated from N_2 adsorption/desorption isotherms determined by relying on an automated nitrogen adsorption analyzer (ASAP 2020, Micromeritics, America), the sample was degassed at 150 °C, keeping for 6 h in vacuum condition before the measurements. The concentrations of the antibiotics solutions after and before adsorption thermodynamic were measured by UV-Vis spectrophotometer (Rang Qi Instrument Technology Co., Ltd, Shanghai, UVG-9PC).

2.4 Adsorption thermodynamic experiments

NFO, OFO and TC were selected as the target antibiotics in the adsorption experiments. A certain mass (1.5~3 mg) of the LAC-AA adsorbents were added into the antibiotics solutions (100 mL) with concentrations varying from 1.0 to 40.0 mg L^{-1}. Typically, the LAC-AA adsorbents were incubated in a certain concentration of antibiotics solutions, and kept stirring at room temperature for different adsorption times. Sample solutions were collected by a 10 mL syringe, followed by filtering through a 0.22 μm Teflon microporous membrane. The concentrations of the sample solutions after a certain period of adsorption was determined by measuring its UV-Vis absorbance. The absolute temperature of the system is under the room temperature (~ 25 °C), the pH value of solutions is kept at 7 during all experiment.

2.4.1 Langmuir and Freundlich isotherms

The adsorption process of the three different antibiotics was fitted to the Langmuir formula which is classical monolayer model as well as the Freundlich that is Multilayer model. The monolayer equation demonstrates the concrete steps about randomly adsorbing antibiotics onto adsorbents' surface. The linearized forms of the Langmuir adsorption formulas are demonstrated as follows [37, 64]:

$$\frac{c_e}{q_e} = \frac{1}{K_L q_m} + \frac{c_e}{q_m} \qquad (1)$$

$$q_e = q_m K_L C_e/(1 + K_L C_e) \qquad (2)$$

C_e stands for the equilibrium concentration (mg L^{-1}), K_L represents the constant of

adsorption (L mg^{-1}), while q_m is the meaning of maximum absorbed capacity by adsorbents (mg g^{-1}), q_e is the values of balanced antibiotics adsorption (mg g^{-1}).

Empirical equation is represented by Freundlich adsorption formula which is simple and commonly used. There is an account of multi-layer adsorption procession, while it means the sites of adsorption which located on surface are not uniform. The basis of multilayer adsorption formula and non-linear model equations areas follows in Equation 3 and 4, respectively [38, 64]:

$$lnq_e = lnK_f + \left(\frac{1}{n}\right) lnC_e \qquad (3)$$

$$q_e = K_F C_e^{1/n} \qquad (4)$$

K_F and n stand for the Freundlich constants [(mg g^{-1}) (L mg^{-1})$^{1/n}$] and adsorption intensity of the adsorbents, respectively. The experimental adsorption isotherms of the LAC-AA adsorbents towards TC, OFO and NFO were fitted to Langmuir (Equation 1-2) and Freundlich isotherm (Equation 3-4) models, respectively.

2.4.2 Adsorption kinetics

The adsorption kinetic mechanisms of three various antibiotics, which were studied in widely research. The pseudo-first-order formula was basis of the assumption that the dominant control of adsorption was diffusion. The pseudo-first-order dynamic formula is given as follows [39, 65]:

$$\mathbf{ln}(\boldsymbol{q_e - q_t}) = \boldsymbol{lnq_e - K_1 t} \qquad \mathbf{(5)}$$

There is a model, which name is pseudo-second-order kinetic, assumes the adsorption rate is determined by the square value about the amount of adsorbed vacancies on the surface of the adsorbent. The dynamic formula of pseudo-second-order is presented as follows [40]:

$$\frac{t}{q_t} = \frac{1}{K_2 {q_e}^2} + \frac{t}{q_e} \qquad (6)$$

q_e stands for the equilibrium adsorption capacity (mg g^{-1}), while q_t is the adsorption capacity (mg g^{-1}) at time t. K_1 is the pseudo-first-order adsorption rate constant, as well as K_2 rate constant of formula (6). The fitting figures of three various antibiotics are

given in Table 3.

2.5 Calculation methods

The calculations of first-principle were applied for relying on the Vienna Ab-initio Simulation Package (VASP) with the Perdew-Burke- Ernzerh (PBE) parameterization of the generalized gradient approximation (GGA) adopted for the exchange correlation potential. [41-42] There is a method whose name is projector augmented wave (PAW), carried for describing the interaction between ions and electrons, [43] and only $1s^1$, $2s^22p^2$, $2s^22p^3$, $2s^22p^4$ and $2s^22p^5$ were regarded as valence electrons for H, C, N, O and F atoms, respectively. Spin-polarized density functional theory was adopted and a 1× 1× 1 Γ-centered k-point mesh was utilized for two meaning including geometry optimization and energy calculation, respectively.[44] Thus, All the geometry optimization was carried out with a conjugate gradient algorithm, while all the energy calculations were carried out with gaussian smearing functions, [45] and the Gaussian smearing parameter was chosen to be σ= 0.02 eV. 500 eV is the concrete figure of basis with the energy cutoff for the plane wave. It is true that the figure of the force on each atom was lower than 0.02 eV $Å^{-1}$.

3. RESULTS AND DISCUSSION

The compositions of the LAC material were measured by XRD, XPS and Raman spectrum. The XRD pattern reveals that the as-obtained LAC material is typically a disordered structure, indicated by the two broadened peaks centered at 23.5° and 43.7°, which are respectively assigned as the (002) and (101) reflection of graphite (Figure 2a). XPS wide scan spectrum suggests that the as-obtained LAC material only has two peak signals, corresponding to C and O elements (Figure S2). After deconvolution, the C 1s signal can be de-convoluted into the C=C/C-C peak at 284.6 eV, the C-O peak at 286.5 eV and the C=O peak at 288.1 eV (Figure 2b). Note that the contents of C-O and C=O are much lower than that of C-C/C=C, demonstrating that the oxidation degree of LAC is very low, consisting with the XRD analysis and the XPS wide scan spectra of

the LAC (Figure S2). To make a comparison, the content of C-O and C=O in the LAC-AA adsorbent is much higher than that of C-C/C=C, illustrating that the large amount of C-O and C=O is from agarose (Figure S3). Raman spectrum also illustrates the successful carbonization of the loofah. As shown in Figure 2c, the figure of G band at ~1603 cm^{-1} reflects the in-plane vibration of sp^2 carbon atoms, while the D band at ~1343 cm^{-1} represents a defect induced Raman feature peak of carbon-based material, implying the non-perfect crystalline structure of the LAC material. The peak intensity ratio of G band to D band (I_G/I_D) is 1.033, indicating that sp^2 domains are the dominant component in the carbon structures which is due to high temperature induced graphitization of loofah. Further, the BET specific surface area of the LAC material was measured by N_2 adsorption/desorption isotherms, as depicted in Figure 2d. As-obtained isotherm is a typical I-V adsorption-desorption curve, demonstrating the microporous structures of the LAC. In addition, the hysteresis loop of the isotherm curve can be classified as a typical H4-type, which reveals that the porous structure of the LAC is similar to the lamellar structure (also known as slit pores). Importantly, from the isotherms, one can figure out that the LAC material possesses a high specific surface area of 736.86 m^2 g^{-1}. Inset of Figure 2d shows the pore size distribution of the LAC, the diameter is around 3.411 nm.

The microscopic structures of the LAC were measured by SEM. As clearly shown in Figure 3a, the LAC consists of a large number of microtubes, suggesting that the macroscopic fibrous-like LAC is actually assembled from one-dimensional porous microstructures (Figure 3b). From high magnification cross-sectional SEM images, one can deduce that the microtubes are uniform with average pore diameters of 20±5 μm，while there are a lot of micropores on the surface of its layered structure (Figure 3b). Interestingly, it is obvious that the microtubes of loofah may be formed by the gradual growth of the helix trestle structures during its growing stage. Besides, two types of helix structures are found in LAC, the red and yellow circles marked in Figure 3c represent the double-helix and single-helix trestle structures, respectively. The average width of the helix fibers is calculated as ~1 μm (upper left inset of Figure 3c). The

enlarged SEM image shows that the surface of the helix fibers is densely occupied by numerous nanoscale protrusions (Figure 3d), which provide abundant active surface sites. Taken together, this unique hierarchical structure (microtubes are assembled from laminae-trestle-laminae (L-T-L) microstructure [46], on which fully covered by nano-protrusions shown in Figure S4 of the LAC contributes significantly to its high specific surface areas, abundant active surface sites and excellent adsorption performances, which will be described hereafter. Importantly, these structures are well maintained in the LAC-AA adsorbent (Figure 4 a-d), which ensures the high-performance adsorption. Moreover, the LAC-AA still exist a large number of microtubes (Figure 4c). Besides, as shown in Figure 4d, the helix structure can be clearly observed.

The LAC-AA adsorbents were incubated in the antibiotics solutions with different concentrations, the incubation time for the adsorption is 140 h, which has been proved to be enough to reach equilibrium. Firstly, as the comparison of the adsorption mass between LAC and LAC-AA adsorbents towards NFO (Table S1), from which one can conclude that the addition of agarose in the LAC material will not affect the adsorption capability, as agarose is a carrier that doesn't have any charged groups, and this is exactly why it has been widely used in analytical chemistry for identifying biological molecules. LAC-AA possesses the super-hydrophilic properties of agarose itself (Figure S5), which accelerates the rate of reaching equilibrium (Table S1).

The fitting parameters, which are based on the isotherms of adsorption in Figure 5, Langmuir and Freundlich formulas (Equation 3-4), are concluded in Table 1. As suggested by the values of R^2, the Langmuir isotherm model is the best fit for the adsorption data that better than the Freundlich model, suggesting the complete monolayer adsorption of antibiotics on the binding sites of the adsorbents. Firstly, the pressure around the atom would increase when the pollutant is adsorbed all the time until the surface of pores has been filled with the molecular, then the balance of adsorption and desorption will appear so that keep the status that the surface sites are filled with monolayer molecular.

From Langmuir model, one can calculate the maximum adsorption capacity (q_m)

of the LAC-AA adsorbents. As listed in Table 1, the (q_m) values of the adsorbents towards TC, OFO and NFO were calculated to be of 537.63, 581.40 and 434.78 mg g^{-1}, respectively. Moreover, there was a good adsorption performance to ppm (1~10 ppm) antibiotics that its maximum adsorption capacity for TC, OFO and NFO was respectively 275, 398 and 310 mg g^{-1} when their equilibrium concentrations are respectively 4.8, 2.2 and 3.0 ppm (Figure S6). Table 2 summarizes the (q_m) values of the currently reported adsorbents from the literatures for the adsorption of TC, OFO and NFO. As seen from Table 2, the LAC-AA adsorbents exhibit the highest (q_m) values compared to currently-available adsorbents. Theoretically, the large adsorption capacity of the LAC-AA adsorbents not only arises from physisorption but also chemisorption. The hierarchical porous structure of LAC should give rise to physisorption, while the aromatic rings of the graphited LAC facilitate the π-π interactions with the antibiotics [47].

Figure 6a shows the adsorption kinetics of TC, OFO and NFO with the initial concentrations of 8 mg L^{-1} by the LAC-AA adsorbents. The adsorption proceeded rapidly within the first 80 h, and gradually slowed down with the increase of the incubation time, and it finally reached the equilibrium after 150 h.

Figure 6b-c illustrates the pseudo-first-order and pseudo-second-order kinetic formulas stick to 3 various antibiotics, while Figure 6d is meaning of the intra-particle-diffusion model. As Table 3 shows, the pseudo-first-order model best described the mechanism of adsorption. Thus, the adsorption step of the adsorbed OFO, TC and NFO by LAC-AA is mainly controlled by diffusion. The concrete formula as follows [22]:

$$q_t = K_{id} t^{1/2} + C \qquad (7)$$

It can be concluded that there are two processes of adsorption: adsorption of adsorbent surface as well as slow pore diffusion. It is the most suitable model (The particle diffusion model) to describe the dynamics of particles in the particle diffusion process [22, 64]. There is a straight line passes which is meaning of particle diffusion is the rate determining step [39, 65]. From Figure 6d, there are three stages of the LAC-AA

296 particle diffusion model which including as follows: the first step is diffusion of the
297 boundary layer, which is mainly the external mass transfer of the adsorbent. Agarose
298 evenly wraps the LAC activated carbon to make the LAC-AA material super
299 hydrophilic (Figure 4, Figure S5). In the first stage, it can quickly contact the surface
300 with nano-scale protrusions for adsorption. Therefore, the main factors of rapid
301 adsorption in the first stage are the super-hydrophilic characteristics of LAC-AA and
302 the adsorption sites of numerous nano-scale protrusions on the surface. After
303 carbonization, the slightly graphitized protuberances on the surface of loofah contact
304 with antibiotic molecules at first, and the π-π bond accumulation of aromatic rings
305 produces the first stage of adsorption.[66] The second stage represents that the internal
306 diffusion of particles is influenced by the microstructure (*eg.* pores) of the adsorbent.
307 The micropores present in the L-T-L microstructure promote the diffusion of the second
308 stage. One of main ways to control the adsorption of antibiotics is filling the pores with
309 size of 2-20 nm, while loofah activated carbon with pore size distribution of 3.41 nm
310 has a favourable structure for absorbing antibiotics. [36] The superior porosity of biochar
311 could offer more adsorption sites for pharmaceuticals molecules, and the micropore
312 could decrease the steric hindrance effect. [67] These two main adsorption steps attract
313 the accumulation of antibiotics under the initial π-π bond accumulation and cooperate
314 with the pore filling effect.[68] The third stage is usually not considered to be a rate-
315 controlling step because of the surface-active adsorption sites and the active sites inside
316 the microspores are all occupied and enter the adsorption equilibrium state. In a word,
317 the three diffusion stages are consistant with the process of monolayer adsorption. In
318 the beginning, the molecular contact the surface with high efficient adsorption, After
319 which, the adsorbed sites become fewer so that the speed of adsorption become slower
320 than before. At last, the balanced status appear and keep the status for a long time.
321 Compared with the adsorption rate of a single LAC adsorbent, the addition of agarose
322 can accelerate the absorption rate of the first stage without affecting the adsorption
323 maximum (Table S1). The atoms or chemical groups on the surface of the biochar can
324 attract the adsorbate to reduce its surface energy. The driving force of adsorption is the
325 sum of many interactions, which contributes to the total free energy of the adsorption

process. [69]

The schematic illustration of the adsorption process of LAC towards OFO is shown in Figure 7a, the L-T-L microstructure has good stability, and this characteristic makes it difficult to change under an oscillating environment. Super hydrophilic of agarose is one beneficial factor for adsorption, while the L-T-L microstructure of LAC and a large number of uniform protrusions on the surface are the main factors affecting the external diffusion of adsorption. Moreover, the micropores with 3.411 nm diameter are the reason for the further diffusion of antibiotics. To understand the adsorption mechanism of these three adsorbates (OFO, TC and NFO), the graphene slab with disorder defects, containing 176 atoms, was used to simulate the amorphous carbon (Figure S7). A vacuum layer of 20 Å was added into two successive slabs to eliminate the interactions between two adjacent slabs. The three atomic adsorption models are shown in Figure 7b (detailed in Figure S8), and the adsorption energies of surface and adsorbates were computed using the following formula [70]:

$$E_{ad} = E_{ads+surf} - (E_{ads} + E_{surf}) \quad (8)$$

Where $E_{ads+surf}$, E_{ads} and E_{surf} are the total energies of the surface with adsorbates, isolated adsorbates and surface, respectively. According to this definition, negative values of E_{ad} indicate the preferential binding of adsorbate to the surface. From the formula for adsorption energy (Equation 8), the E_{ad} were calculated to be of -0.397, -0.629 and -0.385 eV (the calculated results are listed in Table S2) for LAC-TC, LAC-OFO and LAC-NFO, respectively. The probe atom is preferentially adsorbed on the sites with the lowest adsorption energy, [70-71] which means that the adsorbates are prone to be adsorbed on LAC with the order of OFO $<$ TC $<$ NFO. Therefore, the calculated results are in good agreement with the adsorption capacities following the order of OFO $>$ TC $>$ NFO.

The thermodynamics parameters concerning antibiotic adsorption onto LAC-AA, such as Gibbs free energy (ΔG), the solid and liquid phases at equilibrium (K_d), through the following equations can be calculated [72]:

$$K_d = {q_e}/{c_e} \qquad (9)$$

$$\Delta G = -RTIn(K_d) \qquad (10)$$

R is meaning of the universal gas constant (8.314 J mol^{-1} K^{-1}), and 298K is the concrete figure of T in the system (K). Normally, it stands for the physical adsorption is dominant when 0 <ΔG< -20 kJ. mol^{-1}, while the value decreases to it changes to more negative than -40 kJ mol^{-1}, which stands for chemical adsorption is dominant. As shown in Table 4, the calculated result supports the Langmuir formula.

4. CONCLUSIONS

The LAC-AA adsorbents have been facilely fabricated on a large scale, for highly effective removal of antibiotics from contaminated water. Thanks to the unique hierarchical L-T-L microstructures, high specific surface areas and abundant active surface sites of the LAC material, the LAC-AA adsorbents exhibit the largest adsorption capacities towards antibiotics compared to those of currently-available adsorbents. In addition, the LAC-AA adsorbents can effectively improve the circumstance that the water environments were contaminated by multi-level antibiotics (1~40 ppm). This work also encourages us to use naturally occurring products to prepare biosorbents for antibiotics removal from water, which will reduce the cost of the adsorbents and obviate the secondary adverse health effects. The lightweight and compressible properties of the adsorbents ensure their handling and transportation in practical water treatment. Overall, this work should expand new avenues for applying biosorbents in high-performance removal of various antibiotics from water.

ACKNOWLEDGMENTS

The work has been funded by the NSFC (Grant Nos.: 51602193, 21704067, 51701022, 51972055), the Shenzhen Pengcheng Scholar Program, the Shenzhen Science and Technology Research Project (Grant Nos. JCYJ20170818093553012 and JCYJ20180508152903208), the Natural Science Foundation of Hu'nan Province (Grant

No.: 2018JJ3528).

REFERENCES:

[1] A. Sapkota, A. R. Sapkota, M. Kucharski, J. Burke, S. McKenzie, P. Walker, R. Lawrence, Aquaculture Practices and Potential Human Health Risks: Current Knowledge and Future Priorities, Environ. Int. 34(2008)1215-1226.

[2] Y. J. Zhu, J.G. Xie, F. M. Huang, L. Q. Cao, Association between Short-term Exposure to Air Pollution and COVID-19 Infection: Evidence from China, Sci. Total. Environ. 727(2020)138704.

[3] W. F. Yan, Y. Xiao, W. D. Yan, R. Ding, S. H. Wang, F. Zhao, The Effect of Bioelectrochemical Systems on Antibiotics Removal and Antibiotic Resistance Genes: A Review, Chem. Eng. J. 358(2019) 1421-1437.

[4] L. Jiang, S. Jingxiang, C. Xixi, T. Shuang, C. Dingsheng, H. Chun, Efficient Mineralization of Aqueous Antibiotics by Simultaneous Catalytic Ozonation and Photocatalysis using $MgMnO_3$ as a Bifunctional Catalyst. Chem. Eng. J. 358(2019) 48-57.

[5] A. Dirani, I. Mantel, Ranibizumab Treatment History as Predictor of the Switch-response to Aflibercept: Evidence for Drug Tolerance, Clin. Ophthal. 12(2018)593-600.

[6] M. Foroughi, AR. Rahmani, G. Asgari, D. Nematollahi, K. Yetilmezsoy, MR. Samarghandi, Optimization and Modeling of Tetracycline Removal from Wastewater by Three-Dimensional Electrochemical System: Application of Response Surface Methodology and Least Squares Support Vector Machine. Environ. Model. Assess. 25(2020)327-341.

[7] A. Bielen, A. Šimatović, J. Kosićvukšić, I. Senta, M. Ahel, S. Babić, T. Jurina, J. P. González, M. Milaković, N. Udikovićkolić, Negative Environmental Impacts of

Antibiotic-contaminated Effluents from Pharmaceutical Industries, Water Res. 126(2017)79-87.

[8] S. Kim, P. Eichhorn, J. N. Jensen, A. S. Weber, D. S. Aga, Removal of Antibiotics in Wastewater: Effect of Hydraulic and Solid Retention Times on the Fate of Tetracycline in the Activated Sludge Process, Environ. Sci. Technol. 39(2005)5816-5823.

[9] K. Košutić, D. Dolar, D. Ašperger, B. Kunst, Removal of Antibiotics from a Model Wastewater by RO/NF membranes, Sep. Purif. Technol. 53(2007)244-249.

[10] A. J. Watkinson, E. J. Murby, S. D. Costanzo, Removal of Antibiotics in Conventional and Advanced Wastewater Treatment: Implications for Environmental Discharge and Wastewater Recycling, Water Res. 41(2007)4164-4176.

[11] C. L. Amorim, I. S. Moreira, A. S. Maia, M. E. Tiritan, P. M. Castro, Biodegradation of Ofloxacin, Norfloxacin, and Ciprofloxacin as Single and Mixed Substrates by Labrys Portucalensis F11. Appl. Microbiol. Biot. 98(2014)3181-3190.

[12] J. Z. Lyu, J. W. Shao, Y. H. Wang, Y. Q. Qiu, J. Li, T. Li, Y. J. Peng, F. Y. Liu, Construction of a Porous Core-shell Homojunction for the Photocatalytic Degradation of Antibiotics, Chem. Eng. J. 358(2019) 614-620.

[13] P. Liu, H. Zhang, Y. Feng, F. Yang, J. Zhang, Removal of Trace Antibiotics from Wastewater: A Systematic Study of Nanofiltration Combined with Ozone-based Advanced Oxidation Processes, Chem. Eng. J . 240(2014) 211-220.

[14] F. C. Moreira, S. Garcia-Segura, A. R. B. Rui, E. Brillas, V. J. P. Vilar, Degradation of the Antibiotic Trimethoprim by Electrochemical Advanced Oxidation Processes Using a Carbon-PTFE Air-diffusion Cathode and a Boron-doped Diamond or Platinum Anode, Appl. Catal. B-Environ. 160(2014)492-505.

[15] F. Yu, Y. Li, S. Han, J. Ma, Adsorptive Removal of Antibiotics from Aqueous

Solution Using Carbon Materials, Chemosphere. 153(2016)365-385.

[16] N. Le-Minh, S. J. Khan, J. E. Drewes, R. M. Stuetz, Fate of Antibiotics during Municipal Water Recycling Treatment Processes, Water Res. 44(2010)4295-4323.

[17] L.Yu, S. Ruan, X. Xu, R. Zou, J. Hu, One-dimensional Nanomaterial-assembled Macroscopic Membranes for Water Treatment, Nano Today.17(2017)79-95.

[18] D. N. R. D. Sousa, S. Insa, A. A. Mozeto, M. Petrovic, T. F. Chaves, P. S. Fadini, Equilibrium and Kinetic Studies of the Adsorption of Antibiotics from Aqueous Solutions onto Powdered Zeolites, Chemosphere.205(2018)137-146.

[19] M. Brigante, M. E. Parolo, P. C. Schulz, M. Avena, Characterization of Mesoporous Silica Powders and Application to Antibiotic Remotion from Aqueous solution. Effect of Supported Fe-oxide on the SiO_2 Adsorption Properties. Powder Technol. 253(2014)178-186.

[20] P. S. Pinto, T. P. Medeiros, J. D. Ardisson, R. M. Lago, Role of $[FeO_x(OH)_y]$ Surface Sites on the Adsorption of β-lactamic Antibiotics on Al_2O_3 Supported Fe oxide, J. Hazard. Mater. 317(2016)327-334.

[21] J. W. Peterson, L. J. Petrasky, M. D. Seymour, R. S. Bergmans, Laboratory Investigation of Antibiotic Interactions with Fe_2O_3 Nanoparticles in Water, J. Environ. Eng. 142(2016)04016015.

[22] W. Li, J. Wang, G. He, L. Yu, N. Noor, Y. Sun, X. Zhou, J. Hu, I. P. Parkin, Enhanced Adsorption Capacity of Ultralong Hydrogen Titanate Nanobelts for Antibiotics, J. Mater. Chem. A. 5(2017)4352-4358.

[23] C. P. Okoli, A. E. Ofomaja, Degree of Time Dependency of Kinetic Coefficient as a Function of Adsorbate Concentration; New Insights from Adsorption of Tetracycline onto Monodispersed Starch-stabilized Magnetic Nanocomposite, J. Environ. Manage. 218(2018)139-147.

457 [24] J. W. P. Lye, N. Saman, S. S. N. Sharuddin, N. S.Othman, S. S. Mohtar, A. M. M.
458 Noor, J. Buhari, S. C. Cheu, H. Kong, H. Mat, Removal Performance of Tetracycline
459 and Oxytetracycline From Aqueous Solution Via Natural Zeolites: An Equilibrium and
460 Kinetic Study, CLEAN-Soil Air Water. 45(2017)1600260.
461 [25] W. A. Khanday, B. H. Hameed, Zeolite-hydroxyapatite-activated Oil Palm Ash
462 Composite for Antibiotic Tetracycline Adsorption, Fuel. 215(2018)499-505.
463 [26]M. C. Ncibi, M. Sillanpää, Optimized Removal of Antibiotic Drugs from Aqueous
464 Solutions Using Single, Double and Multi-walled Carbon Nanotubes, J. Hazard. Mater.
465 298(2015)102-110.
466 [27] J. Ma, Y. Sun, M. Zhang, M. Yang, X. Gong, F. Yu, J. Zheng, Comparative Study
467 of Graphene Hydrogels and Aerogels Reveals the Important Role of Buried Water in
468 Pollutant Adsorption, Environ. Sci. Technol. 51(2017)12283-12292.
469 [28] D. P. Grover, J. L. Zhou, P. E. Frickers, J. W. Readman, Improved Removal of
470 Estrogenic and Pharmaceutical Compounds in Sewage Effluent by Full Scale Granular
471 Activated Carbon: Impact on Receiving River Water, J. Hazard. Mater. 185(2011)1005-
472 1011.
473 [29] M. Ahmad, A. U. Rajapaksha, J. E. Lim, M. Zhang, N. Bolan, D. Mohan, M.
474 Vithanage, S. S. Lee, Y. S. Ok, Biochar as a Sorbent for Contaminant Management in
475 Soil and Water: a Review, Chemosphere. 99(2014)19-33.
476 [30] Y. Zhuang, F. Yu, J. Ma, Enhanced Adsorption Removal of Antibiotics from
477 Aqueous Solutions by Modified Alginate/Graphene Double Network Porous Hydrogel,
478 J. Colloid. Interf. Sci. 507(2017)250-259.
479 [31] Y. S. Zhang, F. Ali, E. Dervishi, Y. Xu, Z. Li, D. Casciano, A. S. Biris, Cytotoxicity
480 Effects of Graphene and Single-Wall Carbon Nanotubes in Neural
481 Phaeochromocytoma-Derived PC12 Cells, ACS Nano. 4(2010)3181-3186.

[32] A. Pytlak, A. Kasprzycka, A. zafranek-Nakonieczna, SJ. Grzadziel, A. Kubaczynski, K. Proc, P. Onopiuk, A. Walkiewicz, C. Polakowski, A. Galazka, J. Lalak-Kanczugowska, Z. Stepniewska, A. Bieganowski, Biochar Addition Reinforces Microbial Interspecies Cooperation in Methanation of Sugar Beet Waste (pulp), Sci. Total. Environ. 730(2020)138921.

[33] P. P. Liu, Q. R. Wang, C. L. Zheng, C. He, Sorption of Sulfadiazine, Norfloxacin, Metronidazole, and Tetracycline by Granular Activated Carbon: Kinetics, Mechanisms, and Isotherms Water, Air Soil Pollut. 228(2017)129.

[34] M. J. Ahmed, M. A. Islam, M. Asif, B. H. Hameed, Human Hair-derived High Surface Area Porous Carbon Material for the Adsorption Isotherm and Kinetics of Tetracycline Antibiotics, Bioresour Technol. 243(2017)778-784.

[35] H. M. Jang, S. Yoo, Y. K. Choi, S. Park, E. Kan, Adsorption Isotherm, Kinetic Modeling and Mechanism of Tetracycline on Pinus Taeda-derived Activated Biochar, Bioresour. Technol. 259(2018)24-31.

[36] Z. T. Zeng, S. J. Ye, H. P. Wu, R. Xiao, G. M. Zeng, J. Liang, C. Zhang, J. F. Yu, Y. L. Fang, B. Song, Research on the Sustainable Efficacy of G-MoS_2 Decorated Biochar Nanocomposites for Removing Tetracycline Hydrochloride from Antibiotic-polluted Aqueous Solution, Sci. Total. Environ. 648(2019)206-217.

[37] L.Yu, X. Liu, W. Yuan, L. J. Brown, D. Wang, Confined Flocculation of Ionic Pollutants by Poly(l-dopa)-Based Polyelectrolyte Complexes in Hydrogel Beads for Three-Dimensional, Quantitative, Efficient Water Decontamination, Langmuir. 31(2015)6351-6366.

[38] A. H. Ali, Comparative Study on Removal of Cadmium(II) from Simulated Wastewater by Adsorption onto GAC, DB, and PR, Desalin Water Treat. 51(2013) 5547-5558.

[39] X. Fang, S. B. Wu, Y. H. Wu, W. Yang, Y. L. Li, J. Y. He, P. D. Hong, M. X. Nie, C. Xie, Z. J. Wu, K. S. Zhang, L. T. Kong, J. H. Liu, High-efficiency Adsorption of Norfloxacin Using Octahedral UIO-66-NH2 Nanomaterials: Dynamics, Thermodynamics, and Mechanisms, Appl. Surf. Sci. 518(2020)146226.

[40] M. A. Al-Anber, Adsorption Properties of Aqueous Ferric Ion on Natural Cotton Fiber: Kinetic and Thermodynamic Studies. Desalin Water Treat. 52(2014)2560-2571.

[41] G. Kresse, J. Furthmüller, Efficient Iterative Schemes for Ab Initio Total-energy Calculations Using a Plane-wave Basis Set, Phys. Rev. B. 54(1996)11169-11186.

[42] J. P. Perdew, K. Burke, M. Ernzerhof, Generalized Gradient Approximation Made Simple, Phys. Rev. Lett. 77(1996)3865-3868.

[43]G. Kresse, D. Joubert, From Ultrasoft Pseudopotentials to the Projector Augmented-wave Method, Phys. Rev. B. 59(1999)1758-1775.

[44] H. J. Monkhorst, J. D. Pack, Special Points for Brillouin-zone Integrations, Phys. Rev. B. 13(1976)5188-5192.

[45] Sanville, E.; Kenny, S. D.; Smith, R.; Henkelman, G. An Improved Grid-based Algorithm for Bader Charge Allocation, J. Comp. Chem. 28(2007)899-908.

[46] J. K. Huang, J. B. Zeng, H. B. Wang, U. J. Etim, B. Q. Liang, E. B. Meteku, H. Li, Y. Y. Wang, Z. W. Qiu, M. J. Roodd, Z. F. Yan, Biomimetic Fabrication of Highly Ordered Laminae–trestle–laminae Structured Copper Aero-sponge, Nanoscale**.** 16(2020) 8982-8990.

[47] B. Peng, C. Liang, C. Que, Y. Ke, D. Fei, X. Deng, G. Shi, X. Gang, M. Wu, Adsorption of Antibiotics on Graphene and Biochar in Aqueous Solutions Induced by π-π Interactions, Sci. Rep. 6(2016)31920.

[48] D. Shan, S. Deng, C. He, J. Li, H.Wang, C. Jiang, G. Yu, M. R. Wiesner, Intercalation of Rigid Molecules between Carbon Nanotubes for Adsorption

532 Enhancement of Typical Pharmaceuticals, Chem. Eng. J. 332(2018)102-108.
533 [49] B. Li, J. Ma, L. Zhou, Y. Qiu, Magnetic Microsphere to Remove Tetracycline from
534 Water: Adsorption, H_2O_2 Oxidation and Regeneration, Chem. Eng. J. 330(2017)191-
535 201.
536 [50] H. Li, J. Hu, Y. Meng, J. Su, X. Wang, An Investigation into the Rapid Removal of
537 Tetracycline Using Multilayered Graphene-phase Biochar Derived from Waste Chicken
538 Feather, Sci. Total. Environ. 603(2017)39-48.
539 [51] Y. Zhou, X. Liu, Y. Xiang, P. Wang, J. Zhang, F. Zhang, J. Wei, L. Luo, M. Lei, L.
540 Tang, Modification of Biochar Derived from Sawdust and its Application in Removal
541 of Tetracycline and Copper from Aqueous Solution: Adsorption Mechanism and
542 Modelling, Bioresour. Technol. 245(2017)266-273.
543 [52] J. Torres-Pérez, C. Gérente, Y. Andrès, Sustainable Activated Carbons from
544 Agricultural Residues Dedicated to Antibiotic Removal by Adsorption, Chin. J. Chem.
545 Eng.20(2012)524-529.
546 [53] N. Boudrahem, S. Delpeux-Ouldriane, L. Khenniche, F. Boudrahem, F. Aissani-
547 Benissad, M. Gineys, Single and Mixture Adsorption of Clofibric Acid, Tetracycline
548 and Paracetamol onto Activated Carbon Developed from Cotton Cloth Residue Process,
549 Saf. Environ. 111(2017)544-559.
550 [54] X. Mi, M. Wang, F. Zhou, X. Chai, W. Wang, F. Zhang, S. Meng, Y. Shang, W.
551 Zhao, G. Li, Preparation of La-modified Magnetic Composite for Enhanced Adsorptive
552 Removal of Tetracycline, Environ. Sci. Pollut. R. 24(2017) 17127-17135.
553 [55] H. G. Gou, H. N. Wang, Y. Li, L. I. Feng, W. S. Guan, Preparation of Single-cell
554 Carbon Microspheres and Their Use for Adsorption of Tetracycline Hydrochloride, J.
555 B. Univ.Technol. 44(2017)42-48.
556 [56] A. Takdastan, A. H. Mahvi, E. C. Lima, M. Shirmardi, A. A. Babaei, G. Goudarzi,

557 A. Neisi, F. M. Heidari, M. Vosoughi, Preparation, Characterization, and Application of
558 Activated Carbon from Low-cost Material for the Adsorption of Tetracycline Antibiotic
559 from Aqueous Solutions, Water. Sci. Technol. 74(2016)2349-2363.
560 [57] Y. Chen, F. Wang, L. Duan, H. Yang, J. Gao, Tetracycline Adsorption onto Rice
561 Husk Ash, an Agricultural Waste: Its Kinetic and Thermodynamic Studies, J. Mol. Liq.
562 222(2016)487-494.
563 [58] M. H. Marzbali, M. Esmaieli, H. Abolghasemi, M. H. Marzbali, Tetracycline
564 Adsorption by H_3PO_4-activated Carbon Produced from Apricot Nut Shells: A batch
565 Study, Process Saf. Environ. 102(2016)700-709.
566 [59] Y. Zhuang, F. Yu, J. Ma, Facile Synthesis of Three-dimensional Graphene–soy
567 protein Aerogel Composites for Tetracycline Adsorption, J. Chen, Water. Treat.
568 57(2016)9510-9519.
569 [60] L. C. Chen, S. Lei, M. Z. Wang, J. Yang, X. W. Ge, Fabrication of Macroporous
570 Polystyrene/graphene Oxide Composite Monolith and its Adsorption Property for
571 Tetracycline, Chinese Chem. Lett. 27(2016)511-517.
572 [61] B. Huang, D. Xiong, T. Zhao, H. He, X. Pan, Adsorptive Removal of PPCPs by
573 Biomorphic HAP Templated from Cotton, Water. Sci. Technol. 74(2016)276-286.
574 [62] K. W. Goyne, J. Chorover, J. D. Kubicki, A. R. Zimmerman, S. L. Brantley,
575 Sorption of the Antibiotic Ofloxacin to Mesoporous and Nonporous Alumina and Silica,
576 J. Colloid. Interf. Sci. 283(2005)160-170.
577 [63] B.Yan, C. H. Niu, J. Wang, Electron-Donor-Acceptor Interactions, and Site Energy
578 Distribution Analyses of Norfloxacin Adsorption on Pretreated Barley Straw, Chem.
579 Eng. J. 330(2017)1211-1221.
580 [64] B. Wang, X. Xu, H. Tang, Y. Mao, H. Chen, F. Ji, Highly efficient adsorption of
581 three antibiotics from aqueous solutions using glucose-based mesoporous carbon. Appl.

582 Surf. Sci.528 (2020) 147048.
583 [65] W. Y. Gu, X. Y. Huang, Y. H. Tian, M. Cao, L. Zhou, Y. Zhou, J. Lu, J. Y. Lei, Y.
584 B. Zhou, L. Z. Wang, Y. D. Liu, J. L. Zhang, High-efficiency adsorption of tetracycline
585 by cooperation of carbon and iron in a magnetic Fe/porous carbon hybrid with effective
586 Fenton regeneration. Appl. Surf. Sci. 538 (2020) 147813.
587 [66] Q. Chen, X. Wang, P. Zhang, L. J. Zhang, M. Wu, B. Pan, Key roles of electron
588 cloud density and configuration in the adsorption of sulfonamide antibiotics on
589 carbonaceous materials: Molecular dynamics and quantum chemical investigations.
590 Appl. Surf. Sci.536 (2021) 147757.
591 [67] Y. Xiang, X. Yang, Z. Xu, W. Hu, Y. Zhou, Z. Wan, Y. Yang, Y. Wei, J. Yang, D.C.W.
592 Tsang, Fabrication of sustainable manganese ferrite modified biochar from vinasse for
593 enhanced adsorption of fluoroquinolone antibiotics: Effects and mechanisms, Sci Total
594 Environ.709(2020)136079.
595 [68] Z. Zhang, Y. Chen, Z. Wang, C. Y. Hu, D. C. Ma, W. Q. Chen, T. Q. Ao, Effective
596 and structure-controlled adsorption of tetracycline hydrochloride from aqueous solution
597 by using Fe-based metal-organic frameworks. Appl. Surf. Sci. 542 (2021) 148662.
598 [69] R. Zhang, P. Somasundaran, Advances in adsorption of surfactants and their
599 mixtures at solid/solution interfaces. Adv. Colloid Interface Sci. 123(2006)213–229
600 [70] B. C. Han, C. R. Miranda, G. Ceder, Effect of Particle Size and Surface Structure
601 on Adsorption of O and OH on Platinum Nanoparticles: A First-principles Study, Phys.
602 Rev. B. **77**(2008)075410.
603 [71] H. Kim, G. Kim, Adsorption properties of dopamine derivatives using carbon
604 nanotubes: a first-principles study. Appl. Surf. Sci. 501 (2020) 144249.
605 [72] O. Pezoti, A. L. Cazetta, K. C. Bedin, L. S. Souza, A. C. Martins, T. L. Silva,
606 Santos Júnior, O. O. J. V. Visentainer, V. C. Almeida, NaOH-activated Carbon of High

607 Surface Area Produced from Guava Seeds as a High-efficiency Adsorbent for
608 Amoxicillin Removal: Kinetic, Isotherm and Thermodynamic Studies, Chem. Eng. J.
609 288(2016)778-788.
610

Figures and Tables:

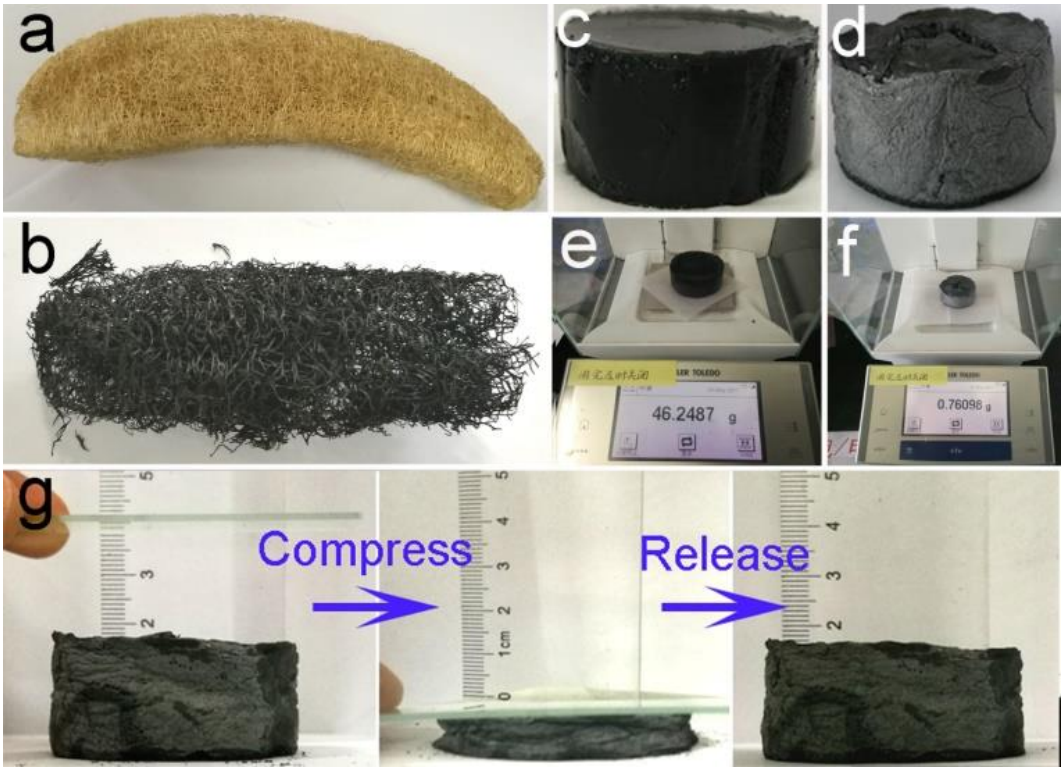

Figure 1 Photographic images of the peeled and naturally-dried loofah (a), the as-obtained loofah activated carbon (LAC) (b), LAC-loaded agarose hydrogel (c) and aerogel (d), respectively. Photographic images showing the weight of the LAC-AA hydrogel (e) and the LAC-AA aerogel (f), respectively. (g) Photographic images showing the intact structures of the LAC-AA adsorbent after compressing and releasing.

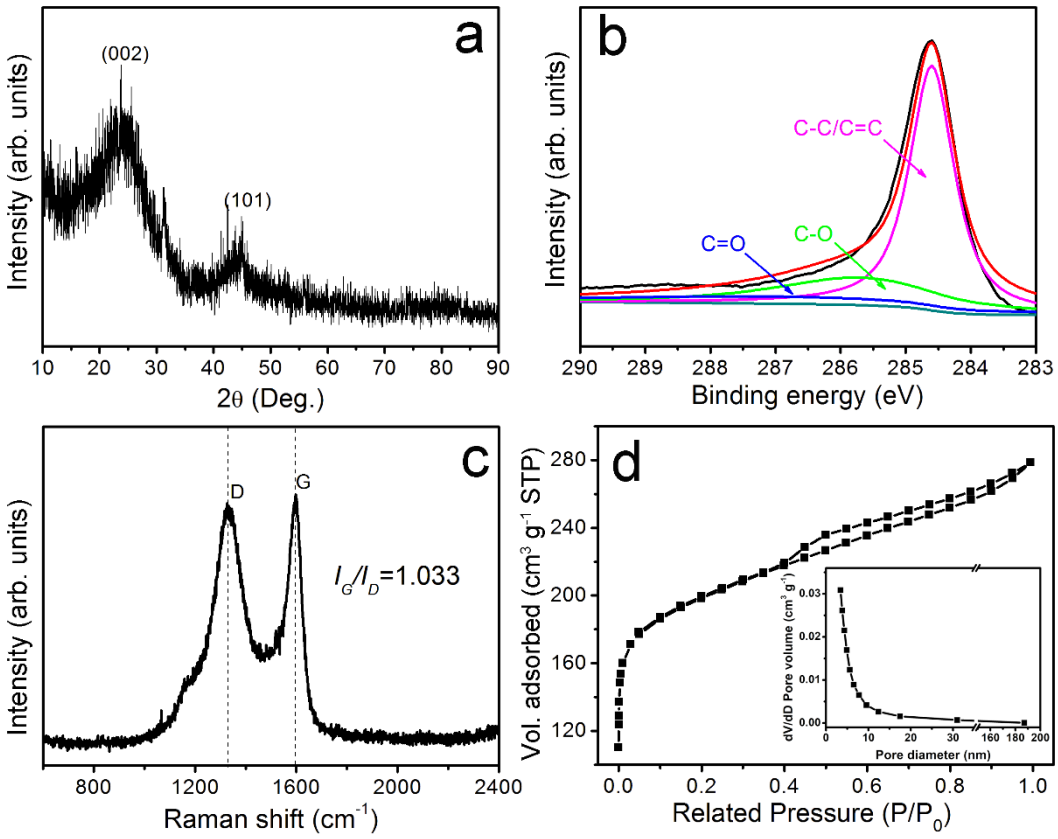

621

622 **Figure 2** XRD pattern (a), high resolution XPS spectra of the C 1s peaks (b), Raman

623 spectrum (c) and Nitrogen adsorption isotherm (d) of the as-prepared LAC.

624

625

626

627

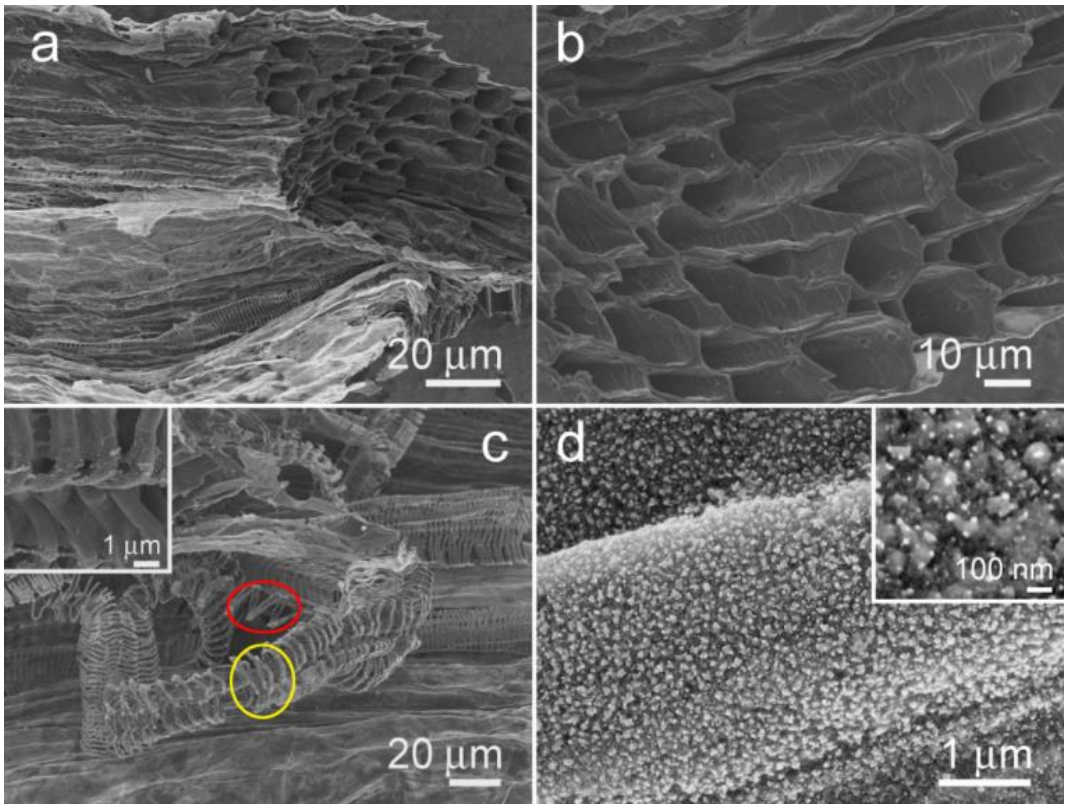

Figure 3 Microstructure characterization of LAC: low (a,c) and high (b,d) resolution SEM images of the LAC. The upper left inset of (c) is an enlarged SEM image of the helix structure. The upper right inset of (d) shows the surface protrusions of the LAC.

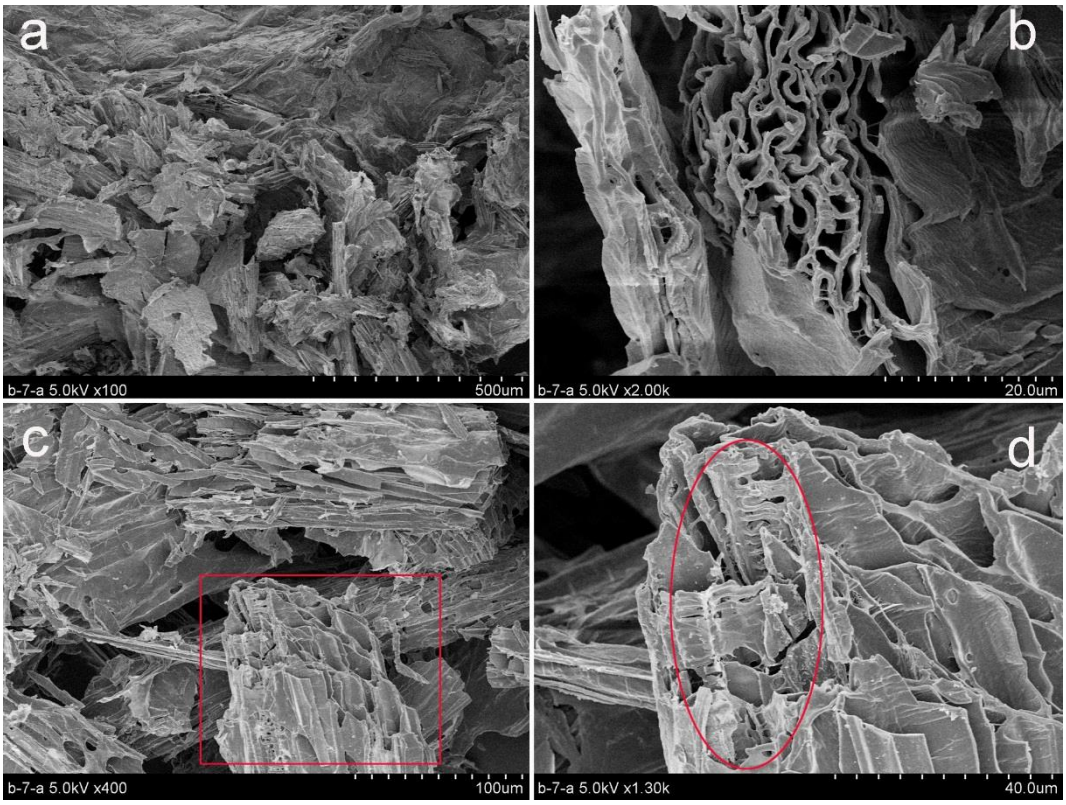

Figure 4 (a-d) Low to high magnification SEM images of as-obtained LAC-AA material.

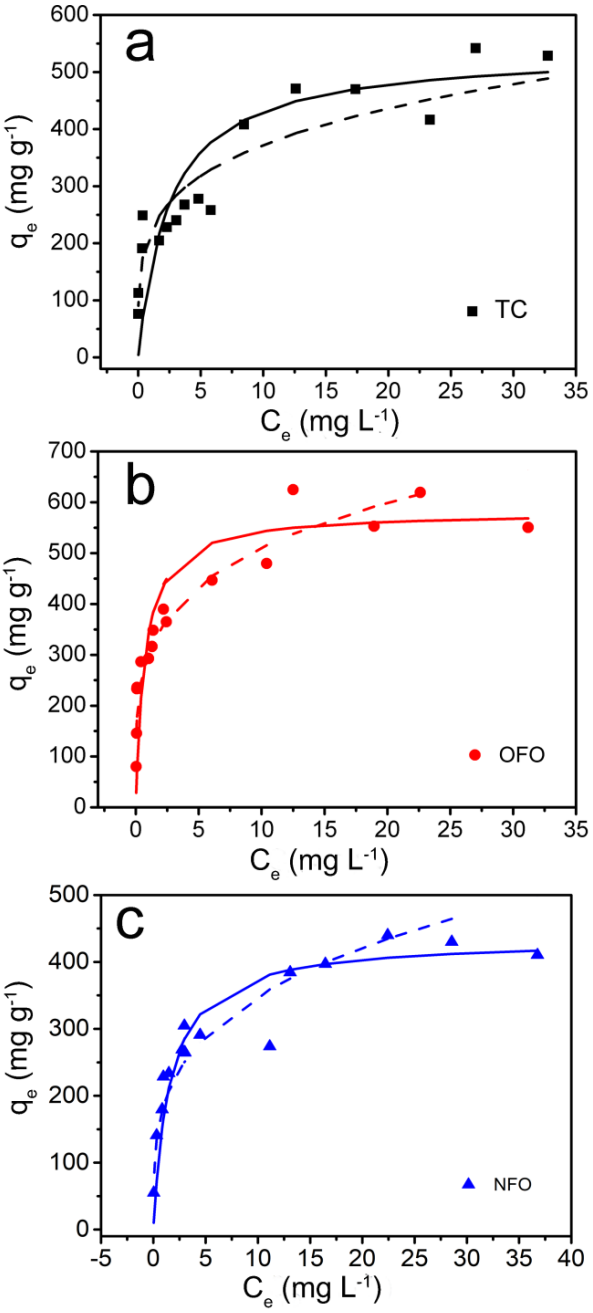

635

636 **Figure 5** The isotherms of adsorption of (1-40 ppm) TC (a), OFO (b) and NFO (c) by
637 the LAC-AA adsorbents, which are fitted by Langmuir (solid curves) and Freundlich
638 models (dashed curves), respectively.

639

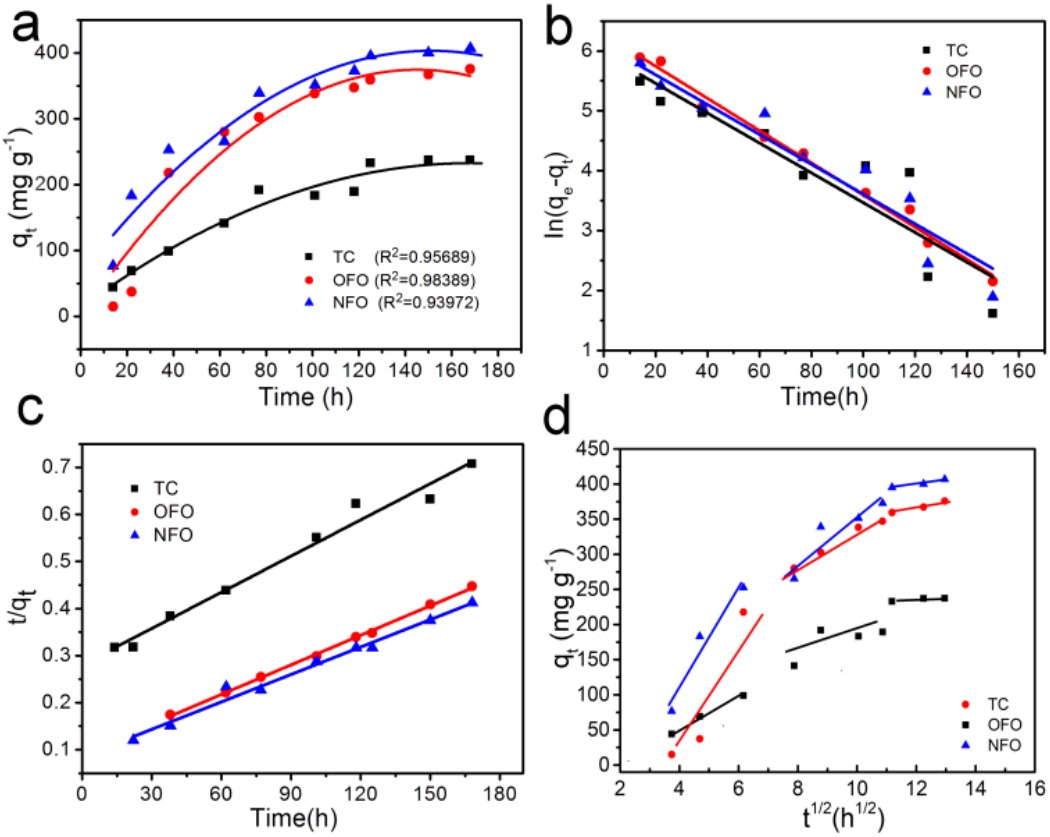

640

641 **Figure 6** (a) The kinetics profiles of adsorption of antibiotics by the LAC-AA
642 adsorbents. (b) The pseudo-first-order model of OFO, TC, NFO. (c) The pseudo-
643 second-order model of OFO, TC, NFO. (d) The intra-particle-diffusion model of OFO,
644 TC, NFO.

645

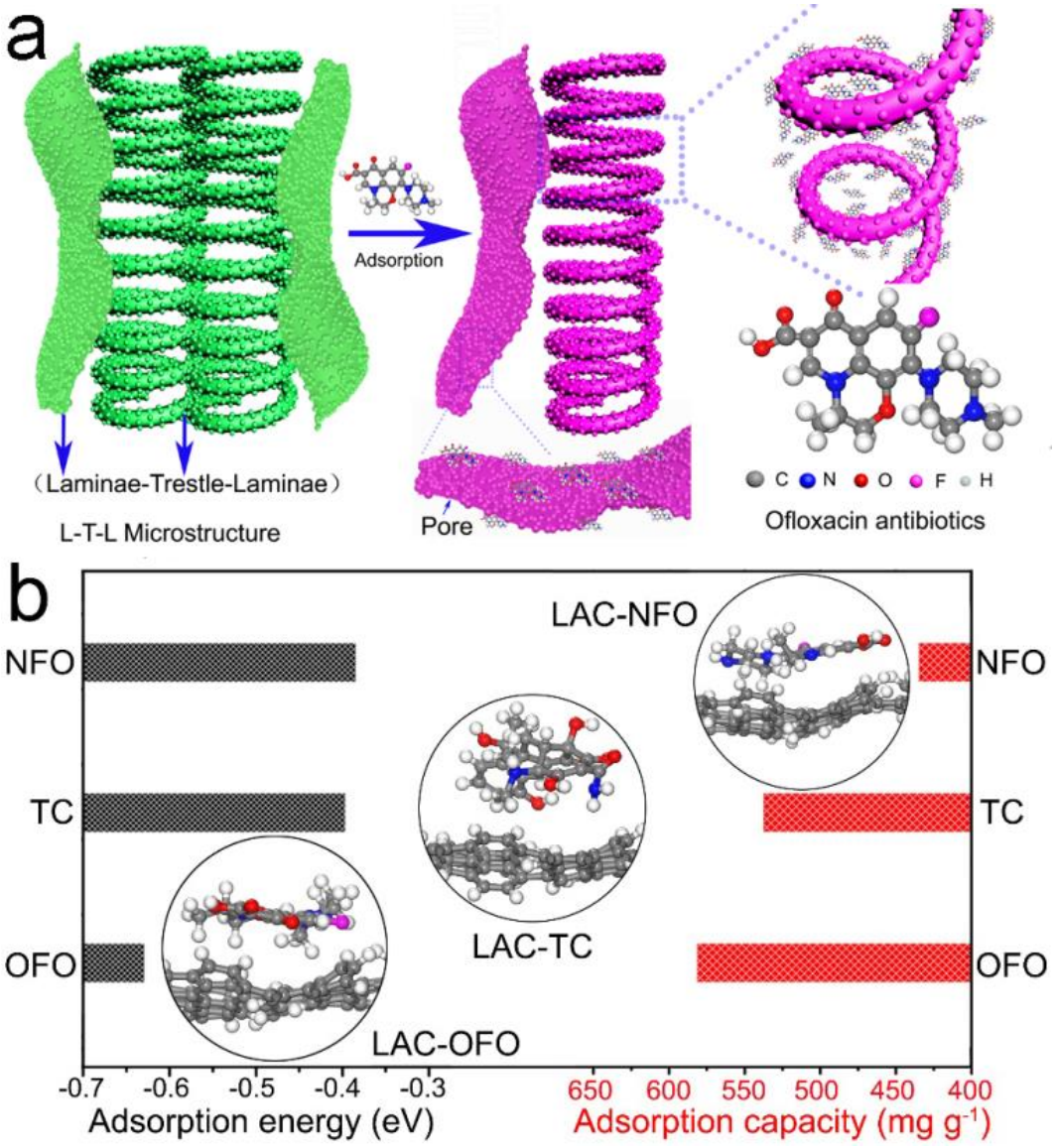

646

647 **Figure 7** (a) Schematic illustration of the adsorption process of LAC towards OFO. (b)
648 The atomic adsorption model for NFO, TC and OFO adsorbed on LAC and the
649 comparison of the corresponding adsorption energy (left axis) and capacity (right axis).
650 The gray, blue, red, pink and white balls represent carbon, nitrogen, oxygen, fluorine
651 and hydrogen atoms, respectively.

652

Tables:

Table 1. Langmuir and Freundlich regression data from the adsorption isotherms of NFO, TC and OFO by the LAC-AA adsorbents.

Isotherm models		Langmuir			Freundlich	
Pollutant	K_L (L mg^{-1})	q_m(mg g^{-1})	R^2	k_f	n	R^2
NFO	0.637	434.78	0.981	185.73	3.658	0.917
TC	0.403	537.63	0.956	220.18	4.374	0.891
OFO	1.398	581.40	0.990	300.49	4.343	0.858

660 **Table 2.** The adsorption capacity comparison of the adsorbent materials

Adsorbents	Antibiotics	q_m (mg g^{-1})	Ref.
Carbon nanotubes (CNTs)	TC	202.67	48
Magnetic microsphere	TC	166	49
Multilayered graphene-phase biochar	TC	388.33	50
Modified biochar derived from sawdust	TC	84.82	51
Human hair-derived porous carbon	TC	128.52	34
AC from beet pulp	TC	288.30	52
Waste textiles	TC	109.00	53
La-modified magnetic composite	TC	145.90	54
GAS composite microspheres	TC	247.52	30
Single-cell carbon microspheres	TC	23.73	55
Zn-AC	TC	282.06	56
Rice husk ash	TC	8.37	57
AC prepared from apricot shell	TC	308.33	58
Graphene-soy protein aerogel	TC	137.00	59
Macroporous polystyrene microsphere/graphene oxide composite	TC	197.90	60
LAC-AA adsorbents	TC	458.00	This work
Biomorphic nano-hydroxyapatite	OFO	29.15	61
Hydrogen titanate nanobelts	OFO	148.14	22
Nonporous SiO_2	OFO	18.70	62
LAC-AA adsorbents	OFO	476.19	This work
Pretreated barley straw	NFO	349.00	63
Octahedral UIO-66-NH_2 nanomaterials	NFO	20.9	39
Hydrogen titanate nanobelts	NFO	111.73	22
LAC-AA adsorbents	NFO	450.45	This work

661

662

663 **Table 3.** Dynamic correlation fitting data of OFO, TC and NFO

	Pseudo-first-order				Pseudo-second-order		
Model	C_0 (mg L^{-1})	K_1 (L min^{-1})	$q_{e,cal}$ (mg g^{-1})	R^2	K_2 (g $mg^{-1}min^{-1}$)	$q_{e,cal}$ (mg g^{-1})	R^2
OFO	8	0.027	535.44	0.988	4.41×10^{-6}	476.19	0.998
TC	8	0.025	386.47	0.840	2.27×10^{-3}	390.63	0.977
NFO	8	0.025	445.84	0.927	3.76×10^{-6}	515.46	0.982

664

665

666

667

668

669 **Table 4.** The values of ΔG calculated by the LAC-AA adsorbing three antibiotics

Pollutant (40 mg L^{-1})	TC	OFO	NFO
q_e (mg g^{-1})	528.35	568.36	402.78
C_e (mg L^{-1})	32.76	31.19	36.75
K_d (L g^{-1})	16.12	18.22	11.16
ΔG (kJ mol^{-1})	-6.88	-7.19	-5.97

670